CrossMark

2-Naphthoic acid ergosterol ester, an ergosterol derivative, exhibits anti-tumor activity by promoting apoptosis and inhibiting angiogenesis

Mingzhu Lin[a], Haijun Li[b], Yan Zhao[a],[*], Enbo Cai[a], Hongyan Zhu[a], Yugang Gao[a], Shuangli Liu[a], He Yang[a], Lianxue Zhang[a], Guosheng Tang[a]

[a] College of Chinese Medicinal Materials, Jilin Agriculture University, Changchun, China
[b] Institute of Translational Medicine, The First Hospital of Jilin University, Changchun, China

ARTICLE INFO

ABSTRACT

Phytosterol is a natural component of vegetable oil and includes ergosterol (ER) and β-sitosterol. In this study, three new ergosterol monoester derivatives were obtained from the reflux reaction with ergosterol, organic acids (furoic acid, salicylic acid, and 2-naphthoic acid), EDCI, and DMAP in dichloromethane. The chemical structures were defined by IR and NMR. On the basis of the results, 2-naphthoic acid ergosterol ester (NE) had the highest tumor inhibition rate and was selected to study anti-tumor activity and its mechanism at doses of 0.025 mmol/kg and 0.1 mmol/kg in H22-tumor bearing mice. Compared with ER, NE exhibited more stronger anti-tumor activity in vivo. Furthermore, biochemical parameters of ALT, AST, BUN, and CRE showed that NE had little toxicity to mice. NE significantly improved serum cytokine levels of IFN-γ and decreased VEGF levels. Moreover, H & E staining, TUNEL assay, immunohistochemistry, and western blotting indicated that NE exhibited anti-tumor activity in vivo by promoting apoptosis and inhibiting angiogenesis. In brief, the present study provided a method to improve ER anti-tumor activity and a reference for a new anti-tumor agent.

1. Introduction

Ergosterol (ER), which exists in yeasts, molds, and most edible and medicinal mushrooms as an important sterol, is the most important chemical raw material and the intermediates of steroid medicine [1–3]; it is used to produce progesterone, cortisone, and other drugs. ER is involved in a variety of important functions in cellular membranes. Structurally, sterols such as ER condense the fluid lipid bilayer by restraining the molecular motion of the phospholipid fatty acyl chains and increase bending rigidity and resistance against area dilation [4,5]. ER is extensively used as an index molecule of living fungal biomass [6]. ER is present in two main forms: free and esterified. The relative abundances would depend on the fungal species. Free ER plays an important role in fluidity, permeability, and integrity of the cell membrane; in addition, this molecule seems to be involved in the effects of membrane-bound proteins associated with nutrient transport and chitin synthesis [7]. However, the ER esters are stored in the hydrophobic core of cytosolic lipid particles and play a role in sterol homeostasis.

Because ER – including fat-soluble and water-soluble ER – has insolubility issues, most pharmacological studies and clinical applications of ER are limited. Therefore, modification of ER into derivatives to enhance pharmacologic activities is a viable method. Most of the modifications thus far have focused on the C3-OH of ER [7]. In the previous study, we synthesized many ER ester derivatives, and their anti-tumor activities in vitro were screened. The results of active screening showed that 2-naphthoic acid esters of ER (NE), furoic acid ergosterol ester (FE), and salicylic acid ergosterol ester (SE) had a relatively strong cytotoxic activity. On the basis of these findings, we conducted a further study on the anti-tumor activities and their mechanisms of ER and its three new monoester derivatives in vivo.

2. Methods and materials

2.1. Chemicals and reagents

ER, furoic acid, 2-naphthoic acid, salicylic acid, 4-dimethylamino-pyridine (DMAP), and 1-ethyl-3-(3-dimethyllaminopropyl) carbodii-

mide hydrochloride (EDCI) were purchased from Sigma-Aldrich (Shanghai) Trading Co., Ltd (Shanghai, China). Cyclophosphamide (CTX) for injection was purchased from Shanghai Huili Biotechnology Co., Ltd. TLC plates were obtained from Qingdao Haiyang Chemical Co., Ltd., and silica gel (200–300 mesh, Qingdao Haiyang Chemical Co., Ltd.) was used for column chromatography. Hematoxylin and eosin (H & E) dye kits were obtained from Nanjing Jiancheng Bioengineering Research Institute (Nanjing, China). TUNEL assay was performed in situ by using the apoptosis detection kit (Roche, Branchburg, NJ, USA) and the DAB detection kit. Interferon-γ (IFN-γ) and vascular endothelial growth factor (VEGF) ELISA kits were purchased from American R & D Co., Ltd. (Minneapolis, MN, USA). ALT (alanine aminotransferase), AST (aspartate transaminase), BUN (blood urea nitrogen), and CRE (creatinine) reagent kits were purchased from Nanjing Jiancheng Bioengineering Institute (Nanjing, China). Rabbit monoclonal anti-Bax, anti-Bcl-2, and anti-VEGF antibodies were purchased from Cell Signaling Technology (Danvers, MA, USA). All other chemicals were of analytical grade from Beijing Chemical Factory.

2.2. Synthesis of compounds

To a solution of 2-naphthoic acid (0.3 mmol) and EDCI (0.4 mmol) in 5 mL dichloromethane stired for 10 min, we added a solution of 0.2 mmol of ER and DMAP (0.2 mmol) in 5 mL dichloromethane. After the solution was heated to reflux for 8 h, the precipitate was removed by filtration, and the solvent was evaporated under reduced pressure. The residue was purified by silica gel chromatography and eluted with petroleum ether/ethyl acetate (5:1, v/v) to yield the product as a light white solid (89.8 mg). The purity of the product was determined as 97.3% by HPLC, and the structure was established by IR and NMR analysis. The other series of ER esters were prepared by a similar procedure.

2.3. Structural determination

The molecular structures of ER esters were identified by ^{1}H NMR and ^{13}C NMR analysis recorded on Varian Mercury 300 MHz NMR spectrometer equipped with a superconducting magnet (Oxford Instruments Ltd., alo Alto, CA, USA). CDCl$_3$ was used as a solvent to dissolve samples, and tetramethylsilane was used as the internal standard for NMR analysis. FTIR analysis of ER esters was performed using a WGH-30A double-beam infrared spectrophotometer (Gangdong Sci & Tech. development Co., Ltd. Tianjin, China).

2.3.1. NE

Yield 79.0%, white powder, C$_{39}$H$_{50}$O$_2$. IR: 3083, 2985–2875, 1725, 1603, 1582, 1505, 1383, 1371 cm^{-1}; ^{1}H NMR (300 MHz, CDCl$_3$) δppm: 8.618 (s, 1H, 1″-H), 8.102 (dd, 1H, J = 1.5,8.7 Hz, 8″-H), 7.973 (dd, 1H, J = 1.2,8.7 Hz, 5″-H), 7.890 (d, 2H, J = 8.7 Hz, 3″,4″-H), 7.611 (ddd, 1H, J = 1.2,8.7,14.4 Hz, 6″-H), 7.588 (ddd, 1H, J = 1.5,8.7,14.4 Hz, 7″-H), 5.649 (m, 1H, 6-H), 5.427 (m, 1H, 7-H), 5.240 (dd, 1H, J = 4.2,7.2 Hz, 22-H), 5.221 (dd, 1H, J = 4.2,7.2 Hz, 23-H), 5.043 (m, 1H, 3-H), 1.075 (d, 3H, J = 6.6 Hz, 21-H), 1.031 (s, 3H, 18-H), 0.956 (d, 3H, J = 6.6 Hz, 28-H), 0.877 (d, 3H, J = 6.9 Hz, 26-H), 0.862 (d, 3H, J = 6.6 Hz, 27-H), 0.657 (s, 3H, 19-H), 2.754 ~ 0.573 (others); ^{13}C NMR (75 MHz, CDCl$_3$) δppm: 165.05 (C1′), 140.47 (C8), 137.45 (C5), 134.52 (C22), 134.41 (C4a″), 131.44 (C8a″), 130.91 (C23), 129.86 (C1″), 128.26 (C8″), 127.06 (C6″), 126.98 (C4″), 126.93 (C5″), 126.68 (C2″), 125.50 (C7″), 124.24 (C3″), 119.30 (C6), 115.31 (C7), 72.50 (C3), 54.64 (C17), 53.47 (C14), 45.00 (C9), 41.78 (C13,24), 39.42 (C20), 37.98 (C12), 36.94 (C1), 36.11 (C10), 35.78 (C4), 32.04 (C26), 27.26 (C2), 27.21 (C16), 21.96 (C15), 20.09 (C11), 19.99 (C26), 18.94 (C27), 18.63 (C21), 16.59 (C28), 15.19 (C18), 11.02 (C19).

2.3.2. FE

Yield 85.2%, white powder, C$_{33}$H$_{46}$O$_3$. IR: 3052, 2972–2884, 1730, 1652, 1384, 1370 cm^{-1}; ^{1}H NMR (300 MHz, CDCl$_3$) δppm: 7.504 (dd, 1H, J = 0.9,1.8 Hz, 5″-H), 7.111 (dd, 1H, J = 0.9,3.6 Hz, 3″-H), 6.441 (dd, 1H, J = 1.8,3.6 Hz, 4″-H), 5.542 (m, 1H, 6-H), 5.334 (m, 1H, 7-H), 5.151 (dd, 1H, J = 4.2,7.2 Hz, 22-H), 5.137 (dd, 1H, J = 4.2,7.2 Hz, 23-H), 4.883 (m, 1H, 3-H), 0.982 (d, 3H, J = 6.6 Hz, 21-CH$_3$), 0.916 (s, 3H, 18-H), 0.860 (d, 3H, J = 6.9 Hz, 28-H), 0.781 (d, 3H, J = 6.9 Hz, 26-H), 0.766 (d, 3H, J = 6.9 Hz, 27-H), 0.565 (s, 3H, 19-H), 2.588–0.479; ^{13}C NMR (75 MHz, CDCl$_3$) δppm: 157.18 (C1′), 145.07 (C5″), 144.06 (C2″), 140.60 (C8), 137.28 (C5), 134.54 (C22), 130.96 (C23), 119.38 (C6), 116.68 (C3″), 115.28 (C7), 110.74 (C4″), 72.53 (C3), 54.69 (C17), 53.50 (C14), 45.02 (C9), 41.80 (C13,24), 39.42 (C20), 38.00 (C12), 36.90 (C1), 36.10 (C4), 35.67 (C10), 32.07 (C25), 27.26 (C2), 27.15 (C16), 21.97 (C15), 20.09 (C11), 20.01 (C26), 18.93 (C27), 18.63 (C21), 16.59 (C28), 15.16 (C18), 11.04 (C19).

2.3.3. SE

Yield 87.9%, light yellow powder, C$_{35}$H$_{48}$O$_3$. IR: 3440, 3080, 2974–2875, 1725, 1674, 1604, 1582, 1382, 1370 cm^{-1}; ^{1}H NMR (300 MHz, CDCl$_3$) δppm: 10.904 (s, 1H, 2″-OH), 7.871 (dd, 1H, J = 1.5,7.8 Hz, 6″-H), 7.477 (dt, 1H, J = 1.8,7.8 Hz, 4″-H), 6.990 (d, 1H, J = 7.8 Hz, 3″-H), 6.904 (dt, 1H, J = 0.9,7.8 Hz, 5″-H), 5.637 (m, 1H, 6-H), 5.421 (m, 1H, 7-H), 5.281 (dd, 1H, J = 4.2,7.2 Hz, 22-H), 5.140 (dd, 1H, J = 4.2,7.2 Hz, 23-H), 5.029 (m, 1H, 3-H), 1.062 (d, 3H, J = 6.6 Hz, 21-CH$_3$), 1.009 (s, 3H, 18-H), 0.940 (d, 3H, J = 6.9 Hz, 28-H), 0.860 (d, 3H, J = 6.6 Hz, 26-H), 0.845 (d, 3H, J = 6.6 Hz, 27-H), 0.649 (s, 3H, 19-H), 2.672–0.562. ^{13}C NMR (75 MHz, CDCl$_3$) δppm: 168.62 (C1′), 160.70 (C2″), 140.71 (C8), 136.99 (C5), 134.51 (C22,C4″), 130.98 (C23), 128.86 (C6″), 119.56 (C5″), 117.98 (C6), 116.51 (C3″), 115.27 (C7), 111.80 (C1″), 73.08 (C3), 54.69 (C17), 53.52 (C14), 45.02 (C9), 41.80 (C13,24), 39.40 (C20), 37.99 (C12), 36.85 (C1), 36.11 (C10), 35.60 (C4), 32.07 (C25), 27.27 (C2), 27.11 (C16), 21.98 (C15), 20.10 (C11), 20.03 (C26), 18.94 (C27), 18.64 (C21), 16.60 (C28), 15.19 (C18), 11.06 (C19).

2.4. Antitumor activity in vivo

2.4.1. Animals and cell lines

Specific Pathogen Free grade, male ICR mice (18–22 g) were purchased from Changchun Yisi experimental Animal Technology Co., Ltd. The mice were kept in the laboratory under aseptic condition: (23 ± 2 °C, 55 ± 5% humidity) on a 12-h light/dark cycle. The mice were provided with a standard pellet diet and water *ad libitum* during the experimental period. Mouse H22-hepatoma cell line was purchased from the Institute of Biochemistry and Cell Biology, SIBS, CAS, Shanghai, China. Murine H22 cells were maintained in the ascitic form by sequential passages into the peritoneal cavities of male ICR mice, as previously described [8].

2.4.2. Tumor-bearing mice model and treatments

A tumor cell suspension of murine H22-hepatoma cells was prepared with physiological saline at a concentration of 1×10^5 cells/mL. The mice were inoculated in the subcutaneous right forelimb armpit with the tumor cell suspension (0.2 mL for each mice) to establish the tumor-bearing mice model. After 24 h, the tumor-bearing mice were randomly divided into five groups, with 8 mice in each group. The mice were intraperitoneally injected with 0.1 mmol/kg body weight of ER, FE, SE, and NE dissolved in soybean oil, respectively (treatment groups), and equal volumes of soybean oil (normal and model groups) 1 time/d for 14 d. The tumor-bearing mice were observed daily and weighed every alternate day. All mice were sacrificed by cervical dislocation. Tumor tissues were excised and weighted. The index of tumor inhibition rate (TIR) was calculated as 100% × (average tumor weight of the control group − average tumor weight of the treatment group)/average tumor weight of the control

ER R=H
SE R=salicylic acid
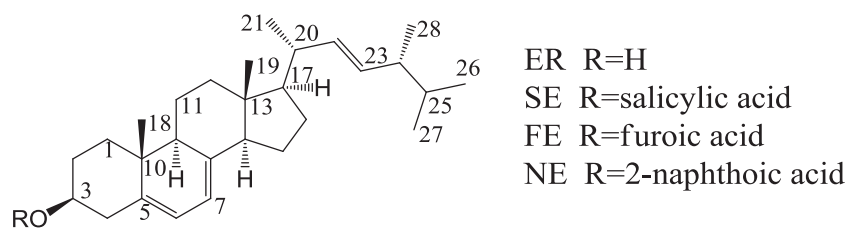FE R=furoic acid
NE R=2-naphthoic acid

Fig. 1. Structures of compound.

Table 1
Effect of ER and its derivatives on tumor weights and tumor inhibition rate.

Groups	TW(g)	TIR (%)
Normal	–	–
Model	1.80 ± 0.13	–
0.1 mmol/kg ER	0.88 ± 0.12**	51.1%
0.1 mmol/kg FE	0.81 ± 0.16**	54.9%
0.1 mmol/kg SE	0.82 ± 0.09**	54.4%
0.1 mmol/kg NE	0.70 ± 0.07**	61.3%

The values are presented as mean ± SD. n = 8, *$p < 0.05$, **$p < 0.01$ compared with the model group.

group. The derivative with the highest TIR continued to be subjected to subsequent experiments.

The subsequent anti-tumor experiments were conducted as follows. The tumor-bearing mice were randomly divided into five groups, with 8 mice in each group. The positive control group was treated with an intraperitoneal injection. The mice were intraperitoneally injected with 25 mg/kg CTX (positive control group), 0.025 mmol/kg, and 0.1 mmol/kg body weight of NE – the derivative with the highest TIR (treatment groups), and equal volumes of soybean oil (normal and model group) 1 time/d for 14 d. The tumor-bearing mice were observed daily and weighed every alternate day. Blood samples were drawn from the eyes of all mice, and they were sacrificed by cervical dislocation. The blood samples were centrifuged to obtained serum for the biochemical assay. Tumor tissues were excised and weighed.

2.4.3. Determination of biochemical parameters

Serum samples of all groups were stored at −80 °C and kept at room temperature to completely melt before the biochemical assay. Four biochemical indexes, including ALT, AST, CRE, and BUN, were determined using commercial reagent kits according to the manufacturer's instructions. In accordance with the procedures described in the commercial kit, IFN-γ and VEGF levels of the mice were determined by indirect ELISA assay.

2.4.4. H & E staining assay

Formalin-fixed tumor and spleen samples were stained with hematoxylin and restained with eosin. The slides were rinsed with water after each step and then dehydrated, cleared, and slide-mounted for final observation. The H & E staining results of the tumor and spleen are shown as color images at 100× and 400× magnification [9].

2.4.5. TUNEL assay

The detection of apoptotic cells of the tumor tissues was performed by the TUNEL assay, with the following modifications [10,11]. Briefly, the tissue sections were treated with 20 mg/mL of proteinase K in distilled water for 10 min at room temperature. To block endogenous peroxidase, the slides were incubated in methanol containing 3% hydrogen peroxide for 20 min, and the sections were then incubated with an equilibration buffer and terminal deoxynucleotidyl transferase. Finally, the sections were incubated with anti-digoxigenin-peroxidase conjugate. Peroxidase activity in each tissue section was indicated by applying diaminobenzidine. The sections were counterstained with hematoxylin.

2.4.6. Immunohistochemistry

Immunohistochemical analysis was performed as previously described [12]. Tumor samples with volumes less than 0.5 cm × 0.5 cm × 0.1 cm were washed with PBS and chosen for immunohistochemical analysis. The analysis was performed after adding normal low-lenthall serum as a blocking fluid to the tissue sections followed by incubation with BAX, Bcl-2, and VEGF. The next day, biotinylated second antibody IgG was added to achieve an antibody binding process, and streptavidin-antibiotin horseradish peroxidase was also added. The staining and restaining experiments were used for DAB and hematoxylin, respectively [12–14].

2.4.7. Western blot

Western blotting is used for qualitative and quantitative analysis of proteins. Qualitative analysis confirms the identity, presence, or absence of a protein or provide a rough estimate of the amounts of a protein [14]. Western blotting was used to analyze the levels of anti-apoptotic factor Bcl-2, the pro-apoptotic factor BAX, and VEGF.

2.4.8. Statistical analysis

All data are presented as mean ± SD. Statistical analysis was performed using SPSS 17.0. t test was used to determine significant differences between the groups.

3. Results and discussion

3.1. Synthesis and structural identification

The ER esterification derivatives (shown in Fig. 1) were obtained by the reaction of ER with organic acids in dichloromethane at 70 °C by reflux. Because water produced during the reaction slows down or even

Table 2
Effects of NE on tumor weight and VEGF and IFN-γ levels.

Groups	TW(g)	TIR (%)	VEGF (pg/ml)	IFN-γ (pg/ml)
Normal	–	–	232.69 ± 23.90	14.76 ± 8.61
Model	1.75 ± 0.16	–	512.75 ± 22.55[bb]	18.44 ± 9.82
CTX	0.60 ± 0.10	68.5%	194.10 ± 38.06[aab]	10.23 ± 3.50[a]
0.025 mmol/kg NE	0.89 ± 0.07[aa]	50.4%	283.48 ± 27.23[aabb]	81.23 ± 6.74[aabb]
0.1 mmol/kg NE	0.68 ± 0.09[aa]	62.0%	273.81 ± 21.15[aabb]	108.80 ± 9.50[aabb]

The values are presented as mean ± SD. n = 8, [aa]$p < 0.01$ and [a]$p < 0.05$ compared with the model group. [bb]$p < 0.01$ and [b]$p < 0.05$ compared with the normal group.

Table 3
Effects of NE on changes in serum biochemistry.

Groups	AST(IU/L)	ALT(IU/L)	CRE(IU/L)	BUN(IU/L)
Normal	12.18 ± 4.89	39.39 ± 9.25	18.02 ± 5.74	11.74 ± 2.08
Model	52.83 ± 11.02[bb]	92.28 ± 8.22[bb]	36.14 ± 8.69[bb]	20.20 ± 3.19[bb]
CTX	71.05 ± 10.21[abb]	104.75 ± 10.69[aabb]	28.86 ± 3.59[abb]	16.16 ± 2.52[aab]
0.025 mmol/kg	24.31 ± 6.66[aabb]	81.05 ± 7.08[aabb]	27.95 ± 7.66[abb]	15.99 ± 0.86[aabb]
0.1 mmol/kg	23.09 ± 3.93[aabb]	60.81 ± 4.23[aabb]	19.22 ± 4.82[aa]	14.48 ± 1.72[aabb]

The values are presented as mean ± SD. n = 8, [aa]$p < 0.01$ and [a]$p < 0.05$ compared with the model group. [bb]$p < 0.01$ and [b]$p < 0.05$ compared with the normal group.
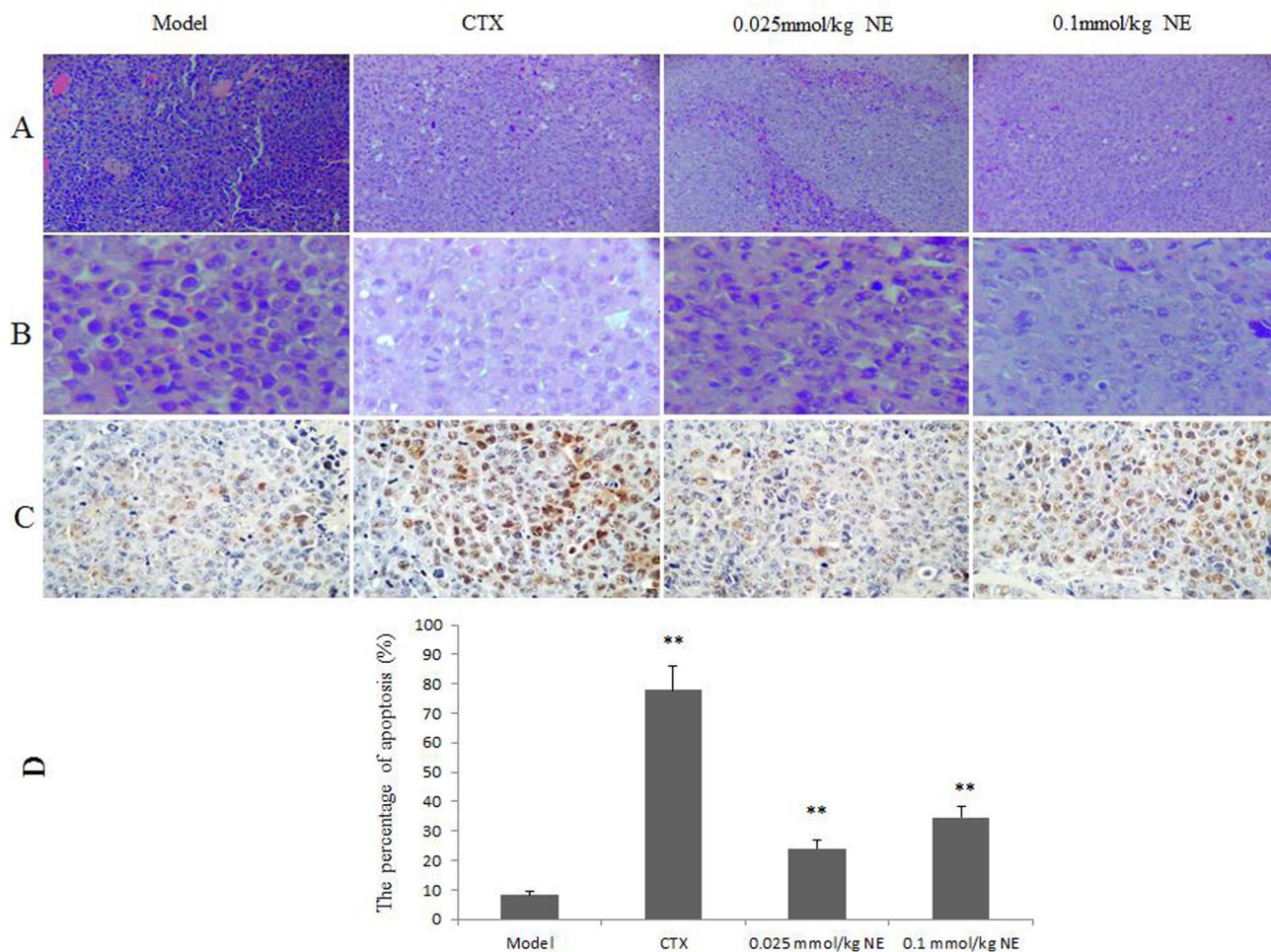

Fig. 2. Histologic examination of morphological changes in tumors from H22-tumor bearing mice. Tumor tissues stained with H & E (100×) (A) and H & E (400×) (B). Tumor sections were analyzed by the TUNEL assay to indicate cell apoptosis (400×) (C) and (D).

stops the reaction, we carried out the reversible process with two molar ratios of EDCI to avoid this side-effect. DMAP (4-dimethylaminopyridine) was used as a catalyst. The products were isolated using a silica gel column. Two methods (FTIR and NMR) were used to identify the molecule structures of synthesized ER esters. The IR absorption spectrum of ER shows an absorption at 1710.7 cm^{-1}, which is from C=O stretch, and the absorption bands at 3342.0–3401.7 cm^{-1} indicate the existence of −O−H (−O−H stretch). For all ER esters, absorption was observed at 1725–1747 cm^{-1} (C=O stretch in moiety of the acyl group), indicating the introduction of an acyl group. The molecular structures of synthesized products were identified by individual ^{1}H NMR analysis, and the characteristic chemical shifts were detailed as follows. In ^{1}H NMR spectrum of all ER esters, the signal at 3.0–6.0 (s, 1H) disappears, indicating that −OH was esterified. The molecular structures of synthesized products were also identified by individual ^{13}C NMR analysis, and the characteristic chemical shifts were detailed as follows. In ^{13}C NMR spectrum of all ER esters, the

signal at 71.6 ppm disappears and re-appear at about 72.00–74.40 ppm, indicating that −OH was esterified, while the signals at 157.18–170.71 ppm indicate the introduction of C=O. Compared with ^{1}H NMR, ^{13}C NMR shows that the esterification reaction was successful.

3.2. Anti-tumor activity

3.2.1. Effect of treatment with ER and its derivatives on tumor weight and TIR

The results of anti-tumor activity of ER and its derivatives in vivo are summarized in Table 1. The table shows that the tumor weight was decreased and the TIR was increased in the H22-tumor-bearing mice treated with ER and its derivatives, and NE showed the highest TIR. NE continued to be subjected to subsequent experiments. The antitumor effect of NE treatment with different doses is shown in Table 2. The results showed that the tumor weight of NE-treated groups was significantly decreased compared that of the model group in a dose-
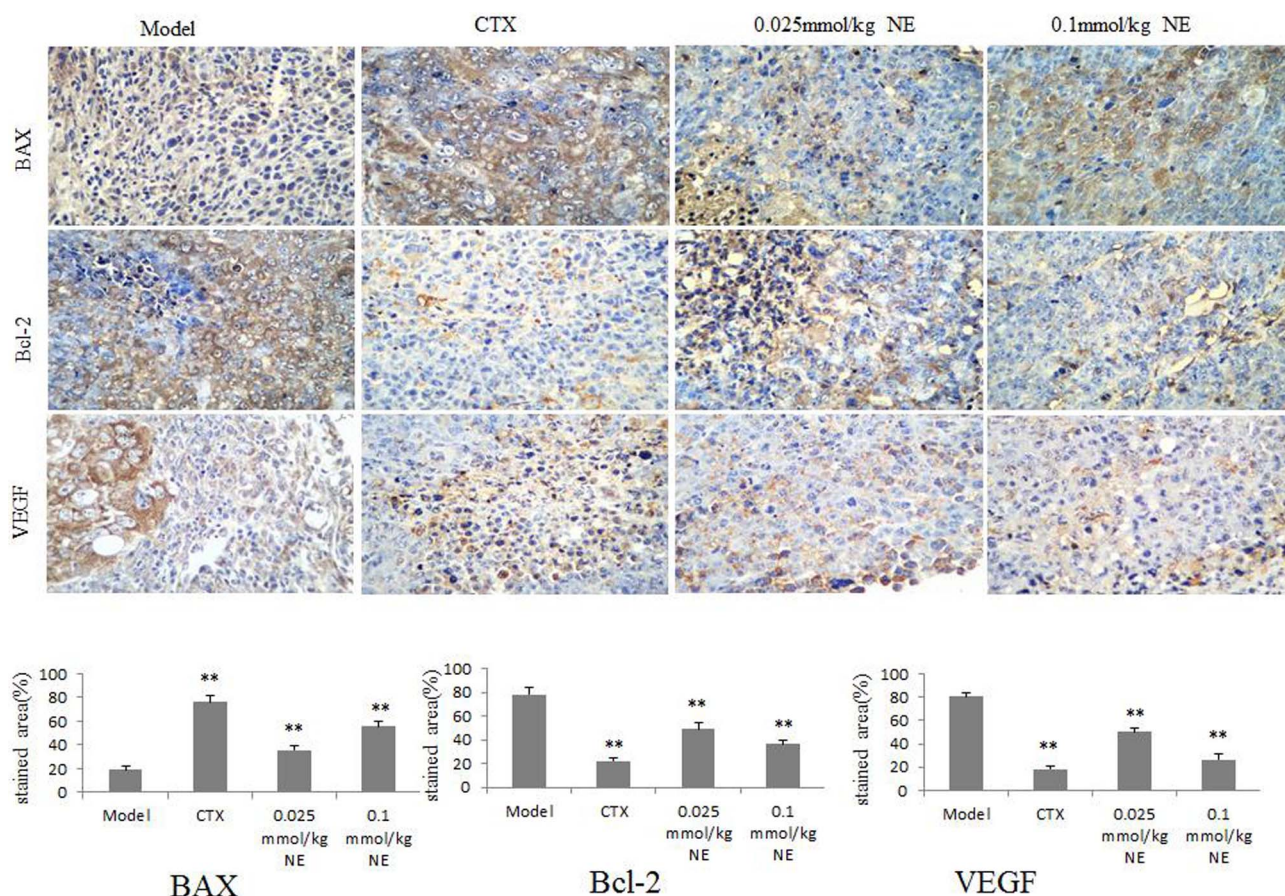
Fig. 3. Immunohistochemical images of tumor tissues and stained area of tumor tissues. The values are presented as mean ± SD, n = 3, **p < 0.01 and *p < 0.05 compared with the model group.

dependent manner, and CTX exhibited the highest TIR.

3.2.2. Effect of NE treatment on the expression of IFN-γ and VEGF

Angiogenesis plays an important role in tumor growth and metastasis; it not only provides the necessary nutrients and oxygen but also removes many metabolic wastes [15]. Several growth factors related to tumor angiogenesis have been identified, including IFN-γ and the VEGF family [16,17]. VEGF can inhibit angiogenesis in the tumor microenvironment [18,19]. VEGFs and their receptors (VEGFRs) play a pivotal role in the formation of both blood and lymphatic vessels in physiological processes (e.g., development, wound healing) and diseases [20,21]. IFN-γ can inhibit cell proliferation [9]. The effects of NE and CTX treatment on the expression of IFN-γ and VEGF are listed in Table 2. As shown in Table 2, treatment with NE increased the serum IFN-γ levels, but decreased the serum VEGF level of mice in a dose-dependent manner. Conversely, the level of IFN-γ was lower in the CTX group than in the model group. VEGF levels were significantly decreased with the treatment of CTX and NE compared with that in the model group.

3.2.3. Effects of NE on changes in serum biochemistry

The ALT and AST values are used to indicate the hepatocellular damage of drugs; the higher the levels, the more is the damage [13]. BUN and CRE levels are the indices of renal injury, and the high content suggests kidney malfunction [22]. The biological changes were measured with serum, and the results are listed in Table 3. The ALT, AST, BUN, and CRE levels of the model group were significantly increased compared with those in the normal control group. Compared with the model control group, the values of these four parameters were significantly decreased in NE-treated groups. However, the ALT and AST levels of the CTX group were significantly increased compared with those of the model group.

3.2.4. Morphological changes after treatment with NE

The tumor pathological sections were stained with H & E and are shown in Fig. 2 (A and B). The nucleus and cytoplasm are shown as blue and pink, respectively. The H & E staining results indicate that tumor cells in the model group were arranged tightly, with a large nucleus and clearly apparent nucleolus. Compared with the model control group, NE at low dose caused few cell deaths, and NE at high dose caused more cell deaths. The effects were comparable to those observed in the CTX group.

Apoptotic cells in tumor cells were tested by TUNEL assay to confirm the inhibitory effect of NE on tumor growth, and brown granules were considered as positively stained [23,24]. The positive cell percentage and pathologic images of the tumor tissues are shown in Fig. 2 (C and D, respectively). The results showed that NE treatment with 0.025 mmol/kg and 0.1 mmol/kg caused an increase in the number of cells undergoing apoptosis compared with that in the model group, and the number of apoptotic cells in the CTX group was most pronounced.

3.2.5. Immunohistochemistry and western blot

BAX, a proapoptotic protein, is cytoplasmic expression, and was shown as brown granules in the immunofluorescent staining (Figs. 3 and 4) [25]. The BAX expression intensities of tumor tissues from NE-treated mice were stronger than those in the model control group, and the expression intensities are shown as the percentage of stained area in Fig. 4, which were significantly increased in tumor tissues of CTX- and NE-treated groups compared to those of the model group (p < 0.01),

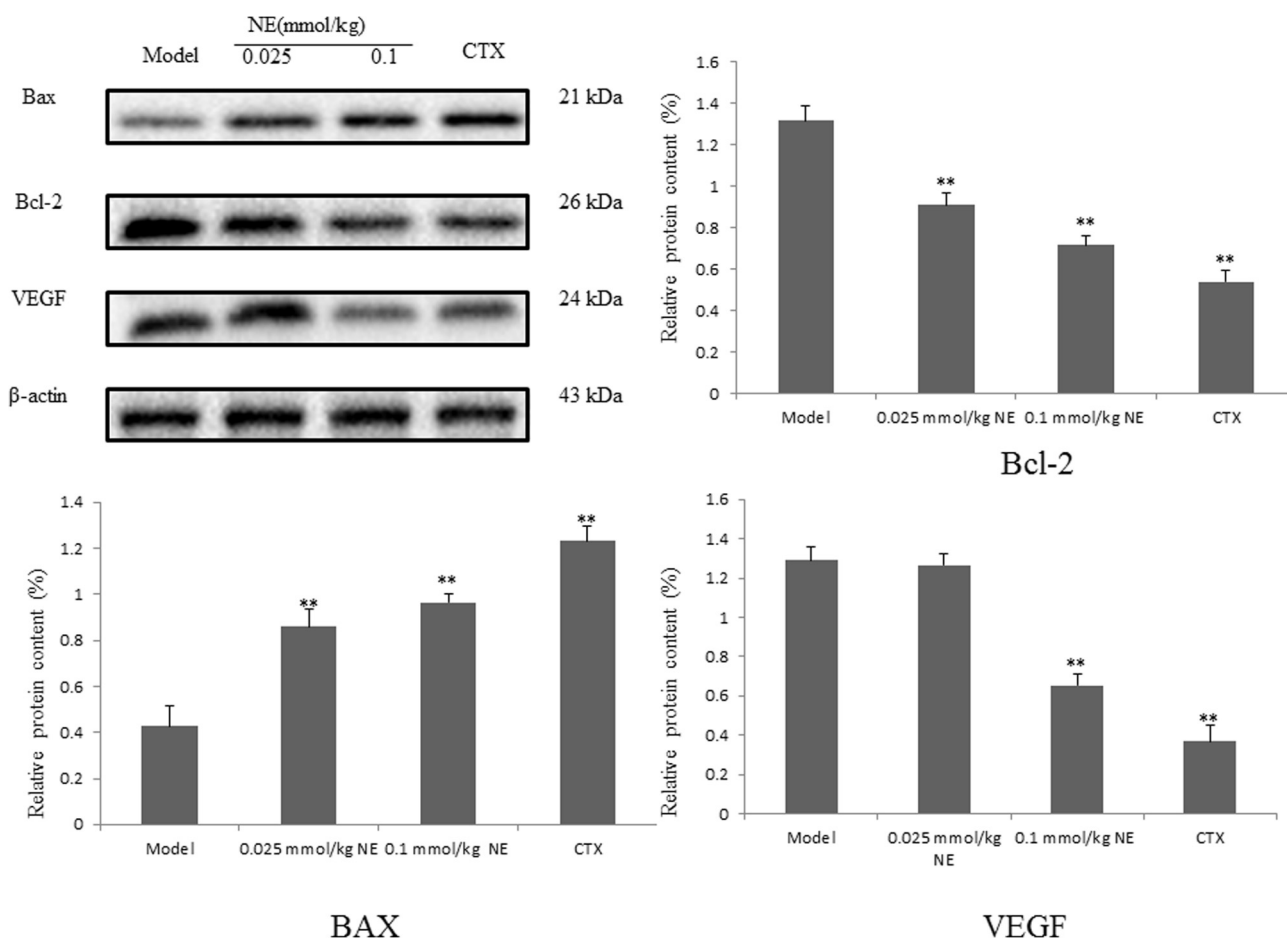Fig. 4. Relative protein expression of BAX and Bcl-2 in tumor tissues. The values are presented as mean ± SD, n = 3, **$p < 0.01$ and *$p < 0.05$ compared with the model group.

CTX treated more expression of BAX than NE. Expression intensities of tumor tissues from the NE high group were stronger than those in the NE low group.

The photographs of Bcl-2 protein expression are shown in Figs. 3 and 4. Bcl-2 is anti-apoptotic protein and plays an important role in apoptosis regulation. Its overexpression causes escape from cell apoptosis [25]. Compared with the model control group, the NE-treated group showed a large decrease in the expression of the Bcl-2 protein. The increased expression of BAX and decreased expression of Bcl-2 cause a decrease in the ratio of Bcl-2 to BAX, which is important for the occurrence of apoptosis [14]. The expression of Bcl-2 in the CTX group was the lowest, and the expression intensity in NE group (0.1 mmol/kg) was similar to that of CTX group.

VEGF is considered as an important growth factor implicated in tumor angiogenesis and can also be used as a tumor marker [26,27]. Photomicrographs of VEGF expression are shown in Figs. 3 and 4. The results showed that VEGF expression in the CTX group was significantly decreased. NE treatment could significantly inhibit the expression of VEGF in a dose-dependent manner, which coincides with the decrease in the VEGF level in serum. The above observation is a hint for the possible role of NE as an angiogenesis inhibitor in H22-tumor bearing mice.

In addition, western blotting was used to analyze the expression of the anti-apoptotic factor Bcl-2, the pro-apoptotic factor BAX, and VEGF. As shown in Fig. 4, the NE-treatment group showed increased expression of the BAX protein and decreased expression of the Bcl-2 protein in the tumor tissue sections ($p < 0.01$), while the protein expression of VEGF in the NE high-dose treatment group was decreased. These results are consistent with those obtained in the immunohistochemical analysis.

4. Conclusions

Our findings indicate that treatment with ER and its derivatives can decrease the tumor weight and increase TIR in H22-tumor-bearing mice, and NE showed better activity in the studied assay. The findings indicated that the intraperitoneal injection of NE increased TFN-γ level and TIR but decreased the serum VEGF level of mice bearing H22 liver cancer. The evaluation of ALT, AST, BUN, and CRE levels in serum showed that NE had low toxic effects on mice. The H & E study of tumors further strengthened the anti-tumor activity of NE, and the Tunel assay results showed that NE can promote the apoptosis of tumor cells. The mechanistic studies showed that NE could stimulate apoptosis through upregulation of the expression of BAX and downregulation of the expression of Bcl-2 and VEGF. Array of studies clearly demonstrate that the molecular mechanisms of the underlying antitumor efficacy of some chemotherapeutic agents are involved in the induction of apoptosis, which is considered to be the preferred measure to treat tumors [13]. As one of the most frequently used antitumor agents for the treatment of a broad spectrum of human cancers, CTX, an anticancer alkylating agent prodrug, is inactive until it is metabolized in the liver by cytochrome P450 to yield phosphoramide mustard and acrolein, which alkylate DNA and proteins, respectively [28]. In the present study, the data of TIR and biochemical changes of serum indicate that the anti-tumor efficacy of NE is close to CTX; but, contrary to CTX damage to the liver, NE exhibits a protective effect on tumor-induced liver injury. Thus, NE, a monoester derivative of ER, with low toxicity and high efficacy as an anti-tumor agent, is a promising chemotherapeutic agent that will be practical in clinical trials and improve the application of NE.

Acknowledgments

References

[1] J.H. Kang, et al., Ergosterol peroxide from Chaga mushroom (Inonotus obliquus) exhibits anti-cancer activity by down-regulation of the beta-catenin pathway in colorectal cancer, J. Ethnopharmacol. 173 (2015) 303–312, http://dx.doi.org/10.1016/j.jep.2015.07.030.

[2] S. Shao, M. Hernandez, J.K. Kramer, D.L. Rinker, R. Tsao, Ergosterol profiles, fatty acid composition, and antioxidant activities of button mushrooms as affected by tissue part and developmental stage, J. Agric. Food Chem. 58 (2010) 11616–11625, http://dx.doi.org/10.1021/jf102285b.

[3] A. Russo, et al., Pro-apoptotic activity of ergosterol peroxide and (22E)-ergosta-7,22-dien-5alpha-hydroxy-3,6-dione in human prostate cancer cells, Chem. Biol. Interact. 184 (2010) 352–358, http://dx.doi.org/10.1016/j.cbi.2010.01.032.

[4] H. Jin, J.M. McCaffery, E. Grote, Ergosterol promotes pheromone signaling and plasma membrane fusion in mating yeast, J. Cell Biol. 180 (2008) 813–826, http://dx.doi.org/10.1083/jcb.200705076.

[5] J. Henriksen, et al., Universal behavior of membranes with sterols, Biophys. J. 90 (2006) 1639–1649, http://dx.doi.org/10.1529/biophysj.105.067652.

[6] J.A. Urbina, New advances in the management of a long-neglected disease, Clin. Infect. Dis. 49 (2009) 1685–1687, http://dx.doi.org/10.1086/648073.

[7] P. Nestel, M. Cehun, S. Pomeroy, M. Abbey, G. Weldon, Cholesterol-lowering effects of plant sterol esters and non-esterified stanols in margarine, butter and low-fat foods, Eur. J. Clin. Nutr. 55 (2001) 1084–1090, http://dx.doi.org/10.1038/sj.ejcn.1601264.

[8] J. Yang, X. Li, Y. Xue, N. Wang, W. Liu, Anti-hepatoma activity and mechanism of corn silk polysaccharides in H22 tumor-bearing mice, Int. J. Biol. Macromol. 64 (2014) 276–280, http://dx.doi.org/10.1016/j.ijbiomac.2013.11.033.

[9] C. Ni, et al., IFN-gamma selectively exerts pro-apoptotic effects on tumor-initiating label-retaining colon cancer cells, Cancer Lett. 336 (2013) 174–184, http://dx.doi.org/10.1016/j.canlet.2013.04.029.

[10] T. Wang, et al., Enhanced tumor delivery and antitumor activity in vivo of liposomal doxorubicin modified with MCF-7-specific phage fusion protein, Nanomed. Nanotechnol. Biol. Med. 10 (2014) 421–430, http://dx.doi.org/10.1016/j.nano.2013.08.009.

[11] H.M. Qu, S.J. Liu, C.Y. Zhang, Antitumor and antiangiogenic activity of *Schisandra chinensis* polysaccharide in a renal cell carcinoma model, Int. J. Biol. Macromol. 66 (2014) 52–56, http://dx.doi.org/10.1016/j.ijbiomac.2014.02.025.

[12] W. Cheng, et al., Induction of interleukin 2 expression in the liver for the treatment of H22 hepatoma in mice, Dig. Liver Dis. 45 (2013) 50–57, http://dx.doi.org/10.1016/j.dld.2012.08.014.

[13] Q. Chen, L. Yang, M. Han, E. Cai, Y. Zhao, Synthesis and pharmacological activity evaluation of arctigenin monoester derivatives, Biomed. Pharmacother. 84 (2016) 1792–1801, http://dx.doi.org/10.1016/j.biopha.2016.10.093.

[14] S.Z. Li, et al., ALLN hinders HCT116 tumor growth through Bax-dependent apoptosis, Biochem. Biophys. Res. Commun. 437 (2013) 325–330, http://dx.doi.org/10.1016/j.bbrc.2013.06.088.

[15] B.L. Hodous, et al., Synthesis, structural analysis, and SAR studies of triazine derivatives as potent, selective Tie-2 inhibitors, Bioorg. Med. Chem. Lett. 17 (2007) 2886–2889, http://dx.doi.org/10.1016/j.bmcl.2007.02.067.

[16] Y. Ito, T. Betsuyaku, K. Nagai, Y. Nasuhara, M. Nishimura, Expression of pulmonary VEGF family declines with age and is further down-regulated in lipopolysaccharide (LPS)-induced lung injury, Exp. Gerontol. 40 (2005) 315–323, http://dx.doi.org/10.1016/j.exger.2005.01.009.

[17] L. Qiu, K. Yoshida, B.R. Amorim, H. Okamura, T. Haneji, Calyculin A stimulates the expression of TNF-alpha mRNA via phosphorylation of Akt in mouse osteoblastic MC3T3-E1 cells, Mol. Cell. Endocrinol. 271 (2007) 38–44, http://dx.doi.org/10.1016/j.mce.2007.03.005.

[18] N.K. Sah, Z. Khan, G.J. Khan, P.S. Bisen, Structural, functional and therapeutic biology of survivin, Cancer Lett. 244 (2006) 164–171, http://dx.doi.org/10.1016/j.canlet.2006.03.007.

[19] S. Jayaram, S. Kapoor, S.M. Dharmesh, Pectic polysaccharide from corn (Zea mays L.) effectively inhibited multi-step mediated cancer cell growth and metastasis, Chem. Biol. Interact. 235 (2015) 63–75, http://dx.doi.org/10.1016/j.cbi.2015.04.008.

[20] N. Ferrara, H.P. Gerber, J. LeCouter, The biology of VEGF and its receptors, Nat. Med. 9 (2003) 669–676, http://dx.doi.org/10.1038/nm0603-669.

[21] T.A. Wilgus, A.M. Ferreira, T.M. Oberyszyn, V.K. Bergdall, L.A. Dipietro, Regulation of scar formation by vascular endothelial growth factor, Lab. Invest. 88 (2008) 579–590, http://dx.doi.org/10.1038/labinvest.2008.36.

[22] J. Fu, et al., Anti-diabetic activities of *Acanthopanax senticosus* polysaccharide (ASP) in combination with metformin, Int. J. Biol. Macromol. 50 (2012) 619–623, http://dx.doi.org/10.1016/j.ijbiomac.2012.01.034.

[23] H. Zhou, et al., The induction of heat shock protein-72 attenuates cisplatin-induced acute renal failure in rats, Pflugers Arch. 446 (2003) 116–124, http://dx.doi.org/10.1007/s00424-002-0996-5.

[24] S.L. Eaton, et al., Total protein analysis as a reliable loading control for quantitative fluorescent Western blotting, PLoS One 8 (2013) e72457, http://dx.doi.org/10.1371/journal.pone.0072457.

[25] A.G. Porter, R.U. Janicke, Emerging roles of caspase-3 in apoptosis, Cell Death Differ. 6 (1999) 99–104, http://dx.doi.org/10.1038/sj.cdd.4400476.

[26] B. Liu, et al., Triptolide downregulates Treg cells and the level of IL-10, TGF-beta, and VEGF in melanoma-bearing mice, Planta Med. 79 (2013) 1401–1407, http://dx.doi.org/10.1055/s-0033-1350708.

[27] S. Fulda, K.M. Debatin, Extrinsic versus intrinsic apoptosis pathways in anticancer chemotherapy, Oncogene 25 (2006) 4798–4811, http://dx.doi.org/10.1038/sj.onc.1209608.

[28] X. Wang, J. Zhang, T. Xu, Cyclophosphamide as a potent inhibitor of tumor thioredoxin reductase in vivo, Toxicol. Appl. Pharmacol. 218 (2007) 88–95, http://dx.doi.org/10.1016/j.taap.2006.10.029.